Materials Research Bulletin 48 (2013) 352–356

Contents lists available at SciVerse ScienceDirect

Materials Research Bulletin

journal homepage: www.elsevier.com/locate/matresbu

Nanostructured columnar heterostructures of TiO_2 and Cu_2O enabled by a thin-film self-assembly approach: Potential for photovoltaics

Özgür Polat [a,b,1], Tolga Aytug [a,*], Andrew R. Lupini [a], Parans M. Paranthaman [a], Mehmet Ertugrul [c], Daniela F. Bogorin [a], Harry M. Meyer [a], Wei Wang [a], Stephen J. Pennycook [a], David K. Christen [a]

[a] Oak Ridge National Laboratory, Oak Ridge, TN 37831, USA
[b] Department of Physics & Astronomy, The University of Tennessee, Knoxville, TN 37996, USA
[c] Atatürk University, Faculty of Engineering, Department of Electric and Electronic Engineering, 25240 Erzurum, Turkey

ARTICLE INFO

Article history:
Received 17 July 2012
Received in revised form 21 September 2012
Accepted 29 October 2012
Available online 6 November 2012

Keywords:
A. Nanostructures
A. Thin films
B. Sputtering
B. Epitaxial growth
D. Microstructure

ABSTRACT

Significant efforts are being devoted to the development of multifunctional thin-film heterostructures and nanostructured material architectures for components with novel applications of superconductivity, multiferroicity, solar photocatalysis and energy conversion. In particular, nanostructured assemblies with well-defined geometrical shapes have emerged as possible high efficiency and economically viable alternatives to planar photovoltaic thin-film architectures. By exploiting phase-separated self-assembly, here we present advances in a vertically oriented two-component system that offers potential for future development of nanostructured thin film solar cells. Through a single-step deposition by magnetron sputtering, we demonstrate growth of an epitaxial, composite film matrix formed as self-assembled, well ordered, phase segregated, and oriented nanopillars of *n-type* TiO_2 and *p-type* Cu_2O. The composite films were structurally characterized to atomic resolution by a variety of analytical tools, and evaluated for preliminary optical properties using absorption measurements. We find nearly atomically distinct TiO_2–Cu_2O interfaces (i.e., needed for possible active *p–n* junctions), and an absorption profile that captures a wide range of the solar spectrum extending from ultraviolet to visible wavelengths. This high-quality materials system could lead to photovoltaic devices that can be optimized for both incident light absorption and carrier collection.

Published by Elsevier Ltd.

1. Introduction

Recently, there has been great interest and progress in the development of controlled, vertically segregated thin film nanocomposites, particularly combinations of oxide systems that, due to the unique structures and interfacial properties, may provide new functionality for a variety of magnetic and electronic phenomena [1,2]. To date, there has been limited work on targeting self-assembled vertical oxide heterostructures for photovoltaic applications. Rather, in recent years the development of planar geometry, single junction thin film solar cells, in particular cadmium telluride (CdTe) and copper–indium–gallium–diselenide (CIGS), has aimed to provide solar energy conversion at lower cost than the established conventional silicon technologies. Presently, CIGS has demonstrated the highest lab-scale cell efficiency at 19.9% [3] with CdTe (16.5%) [4] close behind. However, broad viability is limited by issues associated with low-film qualities, complexity of the manufacturing processes, and scale-up yield. To surmount some of those difficulties and potentially realize higher efficiencies, new approaches such as multi-junction solar cells (with efficiencies of over 40%) [5], dye sensitized solar cells, bulk heterojunctions and organic cells have emerged [6–8]. However, these technologies presently exhibit high manufacturing costs or inadequate efficiencies, poor durability and poor photo-stability, precluding their commercial viability. One of the central issues for low conversion efficiencies in conventional planar *p–n* junction configurations (i.e., thin film multi-layer architectures) is the small minority carrier diffusion length for recombination due to inhomogeneous media, grain boundaries and structural defects (e.g., dislocations, vacancies). On the other hand, nearly one dimensional nanostructured materials including nanorods, nanowires, and nanotubes have been explored as components of photovoltaics (PV) to enable substantial light absorption due to their large surface area and enhanced light trapping capabilities [9–12]. As has been shown on fundamental grounds [13], these nanostructures also have the benefit of requiring only short minority carrier diffusion distances (thereby compensating for short minority carrier lifetimes) and provide efficient spatial carrier separation,

* Corresponding author.
E-mail addresses: aytugt@ornl.gov (T. Aytug), ozgurpolat7@gmail.com (Ö. Polat).
[1] Present address: İstanbul Kültür Üniversitesi, Industrial Engineering Department, E5 Karayolu uzeri, Bakirkoy, 34156 Istanbul, Turkey.

0025-5408/$ – see front matter. Published by Elsevier Ltd.
http://dx.doi.org/10.1016/j.materresbull.2012.10.044

potentially eliminating one of the key limitations of planar device architectures. In effect, a semiconductor device consisting of nanostructures arranged in vertically aligned arrays of radial *p–n* junctions can reduce the occurrence of recombination events and hence may relax the stringent requirements on material quality [9,14,15]. However, despite these attributes PV solar cells based on nanostructured assemblies have yielded poor conversion efficiencies (~0.5–6%) [9,11,16,17]. Possible causes of low efficiencies include non-optimized dimensions and composition, poor density/alignment/ordering of the nanostructures, and low quality heterojunction interfaces. To date, such structures have proven complicated to synthesize at the needed nanoscale, often relying on elaborate techniques that are unsuitably expensive for commercial production.

In this work we demonstrate self-assembled, highly ordered epitaxial nanostructured arrays of TiO_2:Cu_2O, having vertically-aligned interfaces that offer potential to overcome these limitations. Direct band-gap TiO_2 and Cu_2O have been extensively studied as PV materials and photocatalysts for solar energy utilization due to their excellent chemical stability, photostability, non-toxic nature, high abundance and low-cost [18,19], and recent advances were reported in the fabrication of polycrystalline granular or core-shell arrays that exhibited photovoltaic activity, albeit with low efficiency [20,21]. The band gap energies of *n*-type TiO_2 and *p*-type Cu_2O are about 3.2 and 2.1 eV, respectively; these band gaps enable photo-absorption from ultraviolet to the visible region. Furthermore, from a thermodynamic standpoint, the conduction band minimum and valence band maximum of TiO_2 lie below that of Cu_2O, satisfying a key requirement for efficient transfer of both electron and hole minority carriers [19]. Additionally, Cu_2O presents attractive characteristics for photovoltaic devices such as a high optical absorption coefficient and high minority carrier diffusion length as well as relatively good carrier mobility [22,23]. By selecting the TiO_2:Cu_2O system, this study exploits material self-assembly [1,2,24,25], since the component phases exhibit comparatively similar crystal structures [tetragonal-TiO_2 (anatase), cubic-Cu_2O], complete TiO_2–Cu_2O immiscibility, and a lattice parameter difference (~12% misfit) which is suitable for driving the self-assembly. The present method utilizes a simple single step fabrication methodology and demonstrates growth of these unique composite-nanostructured epitaxial-films. This approach could provide a path forward to create highly ordered nanostructured epitaxial film heterostructures with controlled microstructures and low defect concentration that promotes cost-effective fabrication of high efficiency, large-area photovoltaic devices.

2. Experimental details

The deposition of all oxide layers was conducted with an *rf*-magnetron sputtering system. Substrates were prepared by first depositing epitaxial TiO_2 buffer layers on (1 0 0)-surface $LaAlO_3$ (LAO) single crystals, followed by growth of composite TiO_2:Cu_2O films. The sputter targets were prepared from a single-phase anatase TiO_2 (for buffer growth) and a mixture (for composite film growth) of 50 mol% Cu_2O (99.9%, Alfa Aesar) and 50 mol% TiO_2 (99.9%, Alfa Aesar) powders, which were packed into 2 inch diameter copper trays. The sputtering system was initially pumped to a base pressure of 2×10^{-6} Torr and buffer/composite film depositions were carried out in ~5 mTorr argon atmosphere. Epitaxial growth of ~200 nm-thick composite films was established at substrate temperatures of 650 °C and 700 °C, respectively. Substrates were attached to the heater plate using conductive silver paste.

The crystalline quality and phase content of the samples were analyzed by a Philips Model XRG 3100 X-ray diffractometer. Crystallographic texture of the deposited layers were analyzed using a 4-circle X-ray diffractometer employing a Cu source operating at 50 kV and 100 mA and a bent graphite monochromator tuned to Cu K.

The X-ray photoelectron spectroscopy (XPS) examination was carried out to determine the oxidation states of Cu and Ti on and at the near surface of the film. A Thermo Scientific K-Alpha XPS instrument was used to collect data on both as-received as well lightly sputter etched sample surfaces. Monochromatic Al-K_α X-rays were used to collect core level spectra with an electron energy analyzer operating at a pass energy of 50 eV. Ar-ion sputter etching was performed at an ion energy of 3 kV with the sputter gun set at a calibrated etch rate of 15 nm/min on SiO_2 standard films.

Detailed cross sectional examinations of the composite films were conducted by conventional high-resolution transmission electron microscopy and Z-contrast scanning transmission electron microscopy (STEM). The Z-contrast images, with accompanying atomic-resolution electron energy loss spectroscopy (EELS), are sensitive to the atomic species through both the atomic number Z [26] and the EELS absorption edges. The STEM were recorded on a VG Microscopes HB603U fitted with an aberration corrector constructed by Nion Co. (Kirkland, WA), which offers a resolution better than 0.1 nm [27]. Conventional and high resolution TEM was also performed on a FEI CM200-FEG TEM/STEM instrument.

The optical absorbance measurements were performed in reflectance mode by a S.I. Photonics 400 CCD Array ultraviolet-visible (UV-vis) spectrometer. The analysis range was from 350 to 950 nm, and $BaSO_4$ was used as a reflectance standard. Room temperature Hall effect measurements were conducted on sputter deposited planar Cu_2O and TiO_2 films to establish *p*- and *n*-type carrier conductivities, respectively.

3. Results and discussion

Shown in Fig. 1 is a typical $\theta-2\theta$ X-ray diffraction (XRD) pattern of a composite film having nominal TiO_2:Cu_2O concentration, co-deposited from a single sputter target composed of 50 mol% TiO_2 and 50 mol% Cu_2O on a TiO_2-buffered (1 0 0) $LaAlO_3$ (LAO) single crystal substrate. In this substrate architecture, one of the phases (TiO_2) was chosen as a seed layer to simulate future development towards a prototype solar cell module, where the composite matrix should be sandwiched between the two conjugate phases (e.g., one possible architecture for an active module is illustrated in Supplementary Fig. S1). Fig. 1 shows evidence for well-crystallized TiO_2 and Cu_2O phases. The presence of the strong (0 0 *l*) peak reflections of tetragonal anatase-phase TiO_2 and cubic Cu_2O, along with the absence of any additional peak reflections from either TiO_2 or Cu_2O, indicate phase purity and excellent crystallinity, with

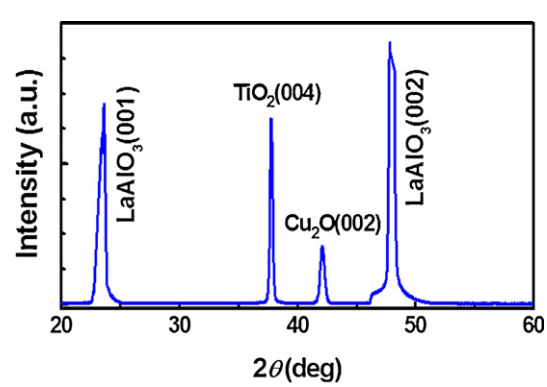

Fig. 1. The $\theta-2\theta$ XRD scan of a mixed phase film with 50 mol% Cu_2O and 50 mol% TiO_2, deposited on TiO_2/$LaAlO_3$. The composite film exhibited preferred *c*-axis orientation. Peak heights of the $LaAlO_3$ reflections were truncated by detector saturation.

the c-axis of both phases aligned normal to the plane of the substrate. The degree of out-of-plane (i.e., c-axis) alignment is determined by the ω-rocking curve scans. The ω-scan full width at half-maximum (FWHM) peak-width values of 0.76°, 0.96° and 0.16° were obtained from the TiO_2 (0 0 4), Cu_2O (0 0 2) and LAO (0 0 2) peak reflections, respectively [see Supplementary Fig. S2(a)–(c)]. The quality of the in-plane epitaxy is determined by the ϕ-scan analysis. Results revealed four equally spaced Cu_2O (1 1 1) and TiO_2 (1 0 1) reflections, separated by 90°, indicating single-domain-oriented growth of each phase as well as an in-plane cube-on cube epitaxy with the TiO_2/LAO substrate [see Supplementary Fig. S2(d)–(e)]. The ϕ-scan FWHM values for the TiO_2 and Cu_2O phases were 0.98° and 1.45°, respectively, and for the LAO (1 1 1) reflection was 0.21°. These comparatively narrow ω- and ϕ-scan peak widths reflect growth of individual segregated phases with direct in- and out-of-plane epitaxy and good single crystallinity.

Supplementary material related to this article found, in the online version, at http://dx.doi.org/10.1016/j.materresbull.2012.10.044.

The elemental composition and chemical state of the composite film surface were investigated by XPS. Data were obtained on the as-received as well as lightly sputter etched sample surfaces. A significant carbon signal was observed on the as-received sample surface (~31 at.%) and is attributed to the accumulation of carbonaceous materials due to atmospheric exposure during the interval between the film deposition and XPS analysis. For the as-received sample, surface composition was Ti = 8.3 at.%; Cu = 15.8 at.%; O = 45.4 at.%; C = 30.5 at.%. After a 30 s Ar-ion sputter etch, the composition changed to Ti = 12.8 at.%; Cu = 35.5 at.%; O = 48.1 at.%; C = 3.6 at.%. The results illustrated in Fig. 2(a) confirm the presence of TiO_2 at the composite surface [28], which showed the Ti $2p_{3/2}$ and Ti $2p_{1/2}$ binding energies at 458.3 and 463.8 eV, implying fully oxidized Ti (Ti^{4+}). A shoulder at lower binding energy (BE) develops with minimal sputtering and indicates the presence of Ti with a lower valence state, due to the sputter etch. In Fig. 2(b); the Cu $2p_{3/2}$ and Cu $2p_{1/2}$ peaks located at 932.4 eV and 952.3 eV show [29] that the copper is present as Cu^+. In addition, a weak satellite feature located at the higher binding energy side (~946 eV) is observed prior and subsequent to surface cleaning, and is attributed to a well ordered Cu_2O phase. Note that the sputter etching alters the satellite-to-main peak area ratio slightly, indicating some disruption of the Cu_2O lattice.

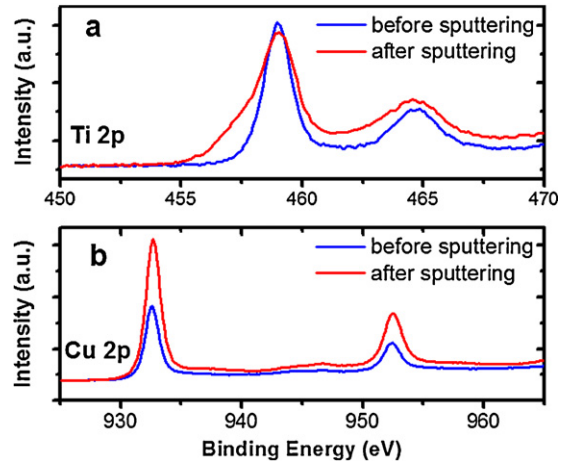

Fig. 2. X-ray photoelectron spectra of a representative composite film surface before and after sputter cleaning. (a) Ti 2p and (b) Cu 2p photoemission signals.

The morphology of the two-phase segregation is revealed in Fig. 3(a), which is a cross-sectional high-angle annular dark field or "Z-contrast" STEM image of a nominal Cu_2O (50 mol%) and TiO_2 (50 mol%) composite film deposited on a TiO_2/LAO template. Note that the higher-Z elements (Cu with Z = 29) appears brighter than the lower-Z elements (Ti with Z = 22) in this imaging mode. The EELS images displayed in the left inset of Fig. 3(a) confirm the segregation of the two phases, where anatase TiO_2 columns of about 20–30 nm width are embedded in a Cu_2O matrix. High resolution plan-view SEM images [Fig. 3(a), inset at lower right] confirm this finding, and show that the TiO_2 phases are indeed columnar, with an areal density of ~3–4 × 10^{10} cm^{-2}, as evidenced by their traces (i.e., darker contrast features) at the film surface. In further considering Fig. 3(a), it appears that the initial phase separation is planar, followed by the formation of vertical pillar TiO_2 structures that begin only after a Cu_2O layer thickness of ~50 nm. Since the buffer layer is TiO_2, it is not possible to discern if an initial TiO_2 phase-separated layer was grown homoepitaxially

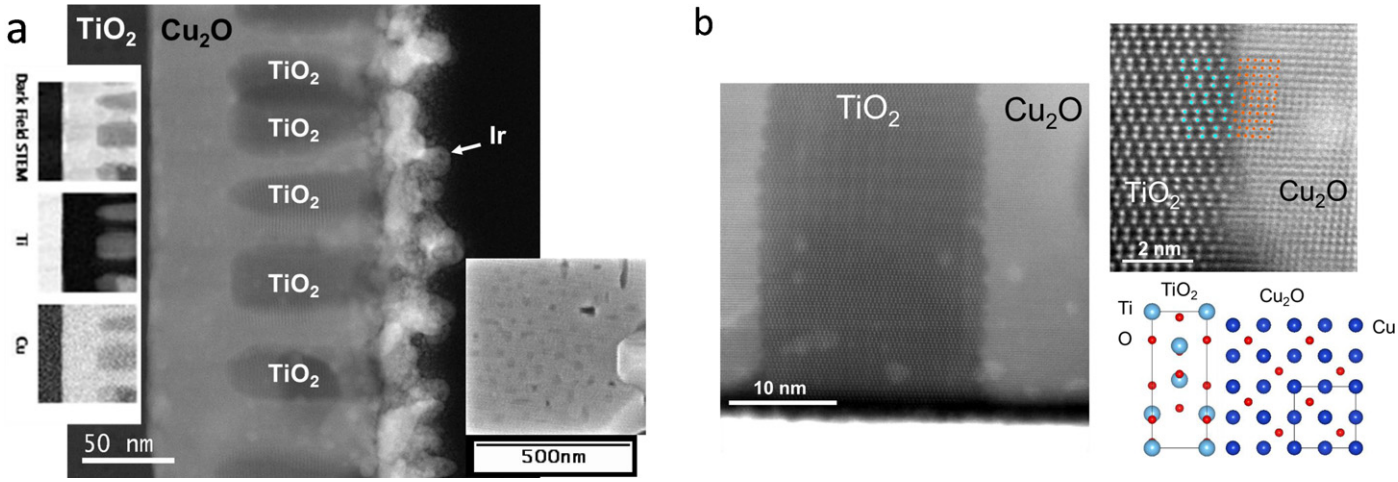

Fig. 3. Cross-sectional microstructures of the nanocomposite film deposited by *rf*-sputtering technique. (a) Z-contrast STEM image of nominal Cu_2O (50 mol%):TiO_2 (50 mol%) on a TiO_2 buffered $LaAlO_3$ substrate, showing the presence of chemically well-separated nanopillar domains of Cu_2O and TiO_2 phases. The Ir layer at the surface is due to the preparation of the samples for microscopy studies. The left inset (not to scale) in (a), Z-contrast dark-field STEM image of a representative region, compared to the Ti and Cu elemental maps obtained using EELS analysis. The bottom right inset is a plan view SEM, showing traces of TiO_2 columns at the sample surface. (b) Low-pass filtered Z-contrast STEM image of the interface between a single crystalline cubic Cu_2O and a single crystalline anatase TiO_2 vertical column. There is no indication of secondary phase formation. A higher magnification image (right panel) shows that the interface between the Cu_2O and TiO_2 phases is nearly atomically sharp. Columns of Ti and Cu atoms near the interface are highlighted with blue and orange colors, respectively. Right lower panel in (c), model structures of TiO_2 and Cu_2O viewed down the [1 0 0] zone axis.

upon the buffer layer, but could be inferred from conservation of mass and the known simultaneous co-deposition impingement of both phases. That is, from the observed ratio of surface phases in the SEM image, the material ratio is inconsistent with the 1:1 target source, but agrees, to within statistical error, with the observed XPS ratios discussed above (i.e., the observed area density and TiO_2 column diameters of ~30 nm correspond to an approximate compositional ratio TiO_2/Cu_2O of ~0.3–0.4). The unusual growth process of layers followed by columns is consistent with the suggestion of Driscoll et al. [2] that the growth mode can be determined by a transition from lateral strain control to vertical (interfacial) strain control, which is expected to occur over a thickness comparable to the resulting vertical column widths. Such a case is a three-dimensional analog of the heterogeneous two-dimensional strain controlled growth of single-phase films by the Stranski-Krastanov growth mode [30]. Here, the switchover is replaced by the self-assembly process which energetically drives nucleation and growth of the TiO_2 phase onto itself in the form of columns propagating normal to the film plane, therefore forming the vertical array structure throughout the upper film thickness. It is noteworthy that in this case the mechanisms dictating the desired phase-separated self-assembly are generally governed by two processes, (i) thermodynamic stability combined with the insolubility between chosen phases (in this case TiO_2 and Cu_2O), driving the phase separation, and (ii) minimization of the elastic strain between the two phases (i.e., lattice misfit, in this case ~12%) and interfacial energies combined with preferential isostructural growth controlling the layer-by-layer vertical self-assembly [2]. A similar growth phenomenon has been observed in $PbTiO_3$-$CoFe_2O_4$ nanostructured system by Tan et al. [31]. In their study, it was shown that the columnar $CoFe_2O_4$ phase starts to grow after a certain thickness of the $PbTiO_3$ matrix, away from the interface. Slutsker et al. [32] have also described this phenomenon by phase-field modeling, which is based on the energy arguments that minimize long-range elastic strain fields. In the present study, the thermodynamic and kinetic conditions were such that phase segregation was observed in all TiO_2:Cu_2O films at temperatures between 650 °C and 760 °C.

The chemical and structural quality of the interfaces is established by high-resolution electron microscopy studies. Fig. 3(b) shows spontaneously ordered, near one dimensional vertical pillar structures within the film matrix, where the observed interfaces at adjacent TiO_2–Cu_2O columns are free of impurity phase inclusions, while exhibiting evidence of periodic faceting. Moreover, atomic-resolution Z-contrast STEM images as displayed in the right panel of Fig. 3(b) reveal that the interface between Cu_2O and TiO_2 pillars is nearly atomically sharp and completely ordered with a periodic lattice misfit. The misfit is observed approximately at a ratio of 10(TiO_2):11(Cu_2O) lattice planes, in close agreement with the lattice mismatch between the two phases (i.e., the ratio of the half TiO_2 *c*-axis with the Cu_2O cubic unit cell). The image was acquired with the axis along the TiO_2 [1 0 0] direction and clearly shows the arrangement of Ti atoms in a dumbbell-like formation. For this zone axis, schematic representation of the crystal structures [33] for TiO_2 and Cu_2O are shown in lower right panel of Fig. 3(b). Such high-quality interfaces, along with the overall single crystal nature, would be very important for fast charge transfer and exciton separation, large minority carrier diffusion lengths, and minimal recombination in the depletion zone. Although no complete cell configuration has yet been constructed, this self-assembled perfection should contribute to high open circuit voltages (V_{OC}), large short-circuit currents (J_{SC}) and good fill factors for improved device efficiencies, while the orthogonalized structure offers the best opportunity to minimize those factors that limit J_{SC} and V_{OC}. For example, the effective series resistance can be reduced due to the short radial charge conduction paths and the shunt resistance maximized by the high crystalline perfection at either side of the interface, which constitutes the depletion zone and will therefore minimize recombination therein.

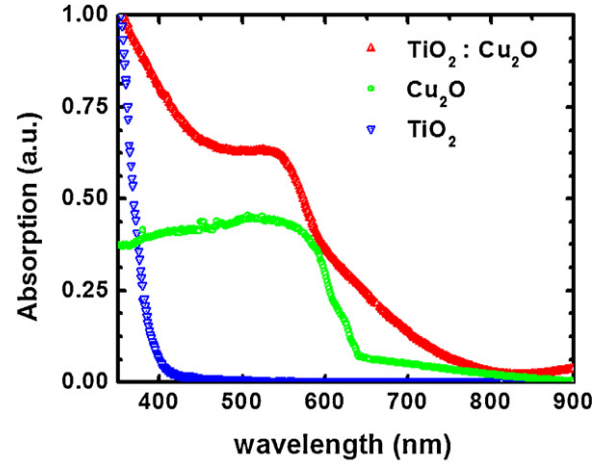

Fig. 4. Representative UV–vis spectrum of a TiO_2:Cu_2O composite film. For comparison, spectra obtained on the TiO_2 and Cu_2O powders, which were used to prepare the sputtering target material, are included.

Basic optical characteristics of the nanopillar structures were investigated by photo absorption measurements using UV–vis spectroscopy. Fig. 4 displays typical absorption spectra of the TiO_2:Cu_2O composite films along with the spectra obtained from the anatase TiO_2 and Cu_2O powders that were used to prepare the sputter target material. Comparison of the individual spectra reveals that the pure TiO_2 powder strongly absorbs only in the UV region with wavelengths shorter than 400 nm, while the Cu_2O powder exhibits strong absorption for wavelengths shorter than 620 nm. These absorption profiles are expected considering the optical band gaps of TiO_2 (~3.2 eV) and Cu_2O (~2.1 eV). On the other hand, the spectrum of the TiO_2:Cu_2O heterostructured film shows two prominent absorption bands in both UV and visible region, which are also related to the characteristic bands of TiO_2 and Cu_2O phases. Note that the absorption profile of the composite film is not a simple sum of TiO_2 and Cu_2O; the absorption edge of TiO_2 red-shifts towards the visible region and the absorption of Cu_2O also extends beyond 620 nm. The integrated absorption feature reveals that the interfaces between the two semiconductors are well coupled. The extended absorption of Cu_2O may originate from some mixed valence of Cu_xO in the film. This net extended absorption range, showing the optical presence of both components, coupled with the observed atomically ordered single-crystalline columnar arrays, motivates further studies on such new classes of nanoscale material systems for potential optoelectronic technologies.

4. Conclusions

As a new concept to the further advancement of oxide thin-film based solar cells, this work offers potential for both improved efficiency and simplified fabrication. The approach invokes single-source composite thin film self-assembly, and the materials offer additional potential benefits, since they are non-toxic, abundant and inexpensive, and highly developed. Moreover, the materials are direct band gap, providing maximum light harvesting over a minimal thickness in thin film form. The epitaxial, crystalline nature of the interfaced assemblies, as demonstrated in this work, should provide additional assurance of large minority carrier diffusion lengths and minimal recombination in the depletion zone, all of which bode well for efficient photovoltaic activity. While good optical absorption characteristics are demonstrated,

further work is needed to demonstrate that these ordered radial interfaces are good photovoltaic *p–n* junctions.

Acknowledgements

T.A. and M.E. were supported by U.S. Department of Energy, Office of Electricity Delivery and Energy Reliability, Advanced Cables and Conductors program and Ö.P. D.K.C., M.P.P., A.R.L., and S.J.P. were supported by the U.S. Department of Energy, Office of Basic Energy Sciences, Materials Sciences and Engineering Division. W.W. was supported by the Laboratory Directed Research and Development Program of Oak Ridge National Laboratory, managed by UT-Battelle, LLC, for the U.S. Department of Energy. D.F.B. acknowledges the support of the ORISE postdoctoral fellowship. XRD and SEM research conducted at the Center for Nanophase Materials Sciences, and Microscopy (A.R.L. and S.J.P.) and XPS (H.M.M.) research conducted at Shared Research Equipment (SHaRE) User Facilities, which are sponsored at Oak Ridge National Laboratory by the Scientific User Facilities Division, Office of Basic Energy Sciences, U.S. Department of Energy.

References

[1] J.L. MacManus-Driscoll, Adv. Funct. Mater. 20 (2010) 2035.
[2] J.L. MacManus-Driscoll, P. Zerrer, H. Wang, H. Yang, J. Yoon, A. Fouchet, R. Yu, M.G. Blamire, Q. Jia, Nat. Mater. 7 (2008) 314.
[3] I. Repins, M.A. Contreras, B. Egaas, C. DeHart, J. Scharf, C.L. Perkins, B. To, R. Noufi, Prog. Photovolt. 16 (2008) 235.
[4] X.Z. Wu, Solar Energy 77 (2004) 803.
[5] R.R. King, D.C. Law, K.M. Edmondson, C.M. Fetzer, G.S. Kinsey, H. Yoon, R.A. Sherif, N.H. Karam, Appl. Phys. Lett. 90 (2007) 183516.
[6] K.H. Yu, J.H. Chen, Nanoscale Res. Lett. 4 (2009) 1.
[7] G.F. Brown, J.Q. Wu, Laser Photonics Rev. 3 (2009) 394.
[8] S. Sista, Z.R. Hong, L.M. Chen, Y. Yang, Energy Environ. Sci. 4 (2011) 1606.
[9] Z.Y. Fan, H. Razavi, J.W. Do, A. Moriwaki, O. Ergen, Y.L. Chueh, P.W. Leu, J.C. Ho, T. Takahashi, L.A. Reichertz, S. Neale, K. Yu, M. Wu, J.W. Ager, A. Javey, Nat. Mater. 8 (2009) 648.
[10] J.A. Czaban, D.A. Thompson, R.R. LaPierre, Nano Lett. 9 (2009) 148.
[11] B.Z. Tian, X.L. Zheng, T.J. Kempa, Y. Fang, N.F. Yu, G.H. Yu, J.L. Huang, C.M. Lieber, Nature 449 (2007) 885.
[12] Y.B. Tang, Z.H. Chen, H.S. Song, C.S. Lee, H.T. Cong, H.M. Cheng, W.J. Zhang, I. Bello, S.T. Lee, Nano Lett. 8 (2008) 4191.
[13] B.M. Kayes, H.A. Atwater, N.S. Lewis, J. Appl. Phys. 97 (2005) 114302.
[14] O.K. Varghese, M. Paulose, C.A. Grimes, Nat. Nanotechnol. 4 (2009) 592.
[15] G.K. Mor, O.K. Varghese, M. Paulose, K. Shankar, C.A. Grimes, Sol. Energy Mater. Sol. Cells 14 (2006) 2011.
[16] E.C. Garnett, P.D. Yang, J. Am. Chem. Soc. 130 (2008) 9224.
[17] C. Colombo, M. Heiss, M. Gratzel, A.F.I. Morral, Appl. Phys. Lett. 94 (2009) 173108.
[18] W. Siripala, A. Ivanovskaya, T.F. Jaramillo, S.H. Baeck, E.W. McFarland, Sol. Energy Mater. Solar Cells 77 (2003) 229.
[19] L. Huang, F. Peng, H.J. Wang, H. Yu, Z. Li, Catal. Commun. 10 (2009) 1839.
[20] D. li, C.-J. Chien, S. Deora, P.-C. Chang, E. Moulin, J.G. Lu, Chem. Phys. Lett. 501 (2011) 446.
[21] Y. Hou, X.Y. Li, Q.D. Zhao, X. Quan, G.H. Chen, Appl. Phys. Lett. 95 (2009) 093108.
[22] A.E. Rakhshani, Solid State Electron. 29 (1986) 7.
[23] A. Mittiga, E. Salza, F. Sarto, M. Tucci, R. Vasanthi, Appl. Phys. Lett. 88 (2006) 163502.
[24] S. Zheng, W.G. Zhu, Y.F. Gao, G.M. Stocks, Z.Y. Zhang, Appl. Phys. Lett. 96 (2010) 71913.
[25] C. Teichert, Phys. Rep. 365 (2002) 335.
[26] S.J. Pennycook, D.E. Jesson, Ultramicroscopy 37 (1991) 14.
[27] P.D. Nellist, M.F. Chisholm, N. Dellby, O.L. Krivanek, M.F. Murfitt, Z.S. Szilagyi, A.R. Lupini, A. Borisevich, W.H. Sides, S.J. Pennycook, Science 305 (2004) 1741.
[28] M.S.P. Francisco, P.A.P. Nascente, V.R. Mastelaro, A.O. Florentino, J. Vac. Sci. Technol. A 19 (2001) 1150.
[29] J. Ghijsen, L.H. Tjeng, J. Vanelp, H. Eskes, J. Westerink, G.A. Sawatzky, Phys. Rev. B 38 (1988) 11322.
[30] M. Ohring, Materials Science of Thin Films, Academic Press, San Diego, 2001, p. 358.
[31] Z.P. Tan, J. Slutsker, A.L. Roytburd, J. Appl. Phys. 105 (2009) 061615.
[32] J. Slutsker, Z.P. Tan, A.L. Roytburd, I. Levin, J. Mater. Res. 22 (2007) 2087.
[33] K. Momma, Izumi F, J. Appl. Crystallogr. 44 (2011) 1272.